Korean Journal of Chemical Engineering (2024) 41:495–501
https://doi.org/10.1007/s11814-024-00037-0

ORIGINAL ARTICLE

Characterization and Formation of Porous Hydroxyethyl Cellulose Membranes via Gas-Based Permeation: A Structural and Thermal Analysis

Heejin Kim[1] · **Sang Wook Kang**[1]

Received: 27 September 2023 / Revised: 24 November 2023 / Accepted: 25 November 2023 / Published online: 15 February 2024

Abstract
This research explores the fabrication of porous Hydroxyethyl Cellulose (HEC) membranes, characterized by their inherent mechanical strength and freedom from additional additives. Employing a gas-based method, a 200-μm HEC film was cast and its permeance was examined under varying gas pressures. The experimental process involved systematic pressure increments, revealing the formation of pores due to solvent evaporation during the drying phase and the subsequent weakening of intermolecular bonds. As gas pressure increased, both the number and size of pores exhibited significant growth, establishing pressure as a critical factor influencing pore characteristics. Structural analysis through Fourier Transform Infrared (FT-IR) spectroscopy demonstrated no chemical alterations during gas permeation, confirming that pore formation was purely a physical phenomenon. FT-IR further identified specific peaks corresponding to the molecular structure of HEC. Deconvolution analysis of the FT-IR data highlighted the absence of chemical changes in the ether and hydroxyl functional groups, reaffirming the physical nature of pore formation. Thermogravimetric Analysis (TGA) was employed to assess thermal stability, revealing that HEC films remained stable even at temperatures exceeding 300 °C. Notably, films subjected to the gas permeation process exhibited more rapid degradation, signifying alterations in their physical properties due to pore formation.

Keywords Hydroxyethyl Cellulose · Battery · Separator

Introduction

Nowadays, batteries have been widely applied in numerous fields. They are prominently utilized in portable electronic devices, energy storage systems, and increasingly in transportation, such as electric vehicles. A battery typically consists of a cathode, an anode, a separator, and an electrolyte, with the separator playing a crucial role in determining both performance of battery and safety during long operation. Positioned between the cathode and the anode, the separator acts as a barrier, preventing electrical short circuits by maintaining a distance between the two electrodes. This separator, functioning as a porous polymer, facilitates the movement of ion charge carriers essential to complete the circuit as the current flows within the cell. The speed of these ion charge carriers is influenced by the wettability of separator to the electrolyte and the structure of the ion transmission pathway, directly affecting the charging rate of the battery [1–12].

For the pivotal role of the separator in battery performance, numerous researchers are actively investigating a wide range of materials, additives, and preparation methods. Polyolefin polymers, including polyethylene (PE) and PP polypropylene (PP), are commonly employed as separator materials. Recent research efforts have been focused on enhancing the stability of medium-sized batteries in response to the increasing demand for electric vehicles, as well as the growing market for lithium-ion batteries (LIBs) and small-scale batteries. In addition to improvements in physicochemical properties, there is a rising interest in environmental considerations, with concerns raised about the treatment and management of waste batteries. Consequently, research on battery recycling technologies is on the rise, and

✉ Sang Wook Kang
swkang@smu.ac.kr

[1] Department of Chemistry and Energy Engineering, Sangmyung University, Seoul 03016, Republic of Korea

the exploration of materials with eco-friendly attributes is gaining much attention [13–18].

Battery separators are categorized into two main types: polyolefin-based and non-polyolefin-based separators. Most separators fall within the polyolefin-based category. The polyolefin separators are characterized by low wettability to electrolytes and limited thermal stability. The manufacturing processes for separator can be broadly classified into wet and dry methods. The wet method relies on an extraction process to create a porous structure, while the dry method is based on a stretching process. A representative approach within the wet process involves phase separation, wherein the polymer is transferred to another phase, leading to the formation of pores. Conversely, the dry method utilizes a vaporization phenomenon, allowing additives or solvents to evaporate without immersing the film in a solvent, thereby generating the pores. On the other hand, the wet method offers advantages such as high mechanical strength, uniform pore distribution, and a straightforward process but is associated with high initial investment costs and low thermal stability. In contrast, the dry method exhibits characteristics that are in contrast to the wet method [19–22].

However, there is continuous need to develop materials for enhancing the stability and cost-effectiveness of battery separators. Polyolefin separators are plagued by significant issues when used in vehicle applications, including non-polarity, low surface energy, and inadequate thermal stability. Thus, there is the potential for lithium-ion batteries (LIBs) to be exploded under accidents [23–25].

Consequently, our research group has recently delved into the exploration of separators employing cellulose acetate (CA) as the primary material. CA polymer has the advantage of possessing remarkable thermal stability while remaining cost-efficient. We employed a hydraulic pressurization method to prepare the separator, resulting in the creation of a straightforward pathway of ion transport. Due to its inherent polymer characteristics, CA exhibits excellent wettability to the electrolyte, facilitating the movement of lithium ions and, subsequently, enhancing charging speeds. Through a series of comprehensive analyses, we have established the numerous advantages of CA, thereby anticipating various applications in the field of porous materials [26].

However, CA has a challenge concerning its mechanical strength due to its relatively low molecular weight. This limitation can be mitigated by combining it with PP and PE, materials known for their higher mechanical strength. Simultaneously, CA can improve the hydrophobic properties of PP and PE to compensate for their limited affinity, yielding a complementary film. The production of a porous CA polymer necessitates the addition of plasticizers like glycerin and lactic acid to enhance flexibility. However, the prepared CA by glycerin and lactic acid shows relatively low mechanical properties due to their low molecular weight.

Thus, our study focuses on the development of a separator using hydroxyethyl cellulose (HEC) with a higher mechanical property than CA to address its low mechanical strength. HEC exhibits limited solubility in organic solvents but is readily dissolved in distilled water. HEC is known for enhancing structural strength and viscosity and is employed in paint, coating formulations, and widely applied in the oil and gas industries as an additive. Thus, neat HEC solution is notably viscous, and when converted into a film, it yields a flexible yet mechanically robust product due to its inherent properties.

We initiated our research by manufacturing pure HEC membranes without additional additives. Through gas permeation, we observed the formation of pores in the HEC polymer, achieved by a pressurization process using gas. Owing to its characteristics, HEC exhibits a high affinity to electrolytes, leading to expectations of fast charging and discharging rates. Moreover, it proves to be an economically viable option, as it utilizes readily available distilled water as a solvent, eliminating the need for supplementary additives. HEC, depending on the specific material requirements for polymer film and the applied pressurization process, holds the potential for mass production, making it a promising technology in the competitive battery market that aligns with environmental considerations.

Materials and Methods

Materials

2-Hydroxyethyl cellulose (HEC, average Mw ~ 90,000 g/mol) was purchased from Sigma-Aldrich Co., Ltd., USA. Acetone (99.8%) was purchased from Daejung chemicals and metals Co., Ltd., Seoul, Korea.

Methods

Preparation of Porous HEC

To prepare a 10-g solution containing 3-wt% hydroxyethyl cellulose (HEC), a solvent mixture by combining 1.94 g of acetone and 7.76 g of distilled water (acetone:distilled water = 2:8 wt%) is prepared. Then, 0.300 g of HEC is added to the solvent and stir the mixture for 24 h. When preparing a 3-wt% HEC film, prolonged stirring revealed that water-soluble HEC underwent chemical decomposition when in contact with water. On the other hand, when stirred for a shorter duration, the binding strength in regions where HEC was not thoroughly dissolved remained weak, indicating inadequate dispersion.

It was observed that altering the ratios of distilled water and acetone resulted in difficulties when attempting to cast

HEC into film form. Increasing the proportion of distilled water appeared to cause decomposition, while increasing the acetone ratio led to non-uniform dissolution and excessive cohesion, making casting impossible. The solution was then applied onto a glass plate using a 200-µm Doctor blade and dried in a thermostat at 25 °C with 50% humidity for 1 h. The resulting film, transparent and thin, exhibited strong adhesion to the glass plate. Subsequently, the film was peeled off the glass plate using adhesive tape.

The mechanical strength of HEC film was evaluated by subjecting it to a gas flux method, raising and stabilizing the pressure from 0.5 bar to 3.5 bar, with each pressure level maintained for 20 min. The HEC film demonstrated robust mechanical properties, even under high-pressure conditions. Gas flux data are presented in gas permeation unit (GPU = 1×10^{-6} cm^3 (STP)/(cm^2 s cmHg)).

Analysis

Following casting, the membrane obtained through the gas cell system underwent a drying period of at least 3 days under vacuum conditions. It was then subjected to specific analytical procedures to identify and compare physicochemical changes against reference values. Surface analysis of the separators was conducted using a scanning electron microscope (SEM, JSM-5600LV, JEOL, Tokyo, Japan). Fourier transform infrared spectroscopy (FT-IR, VERTEX 70/70 V FT-IR spectrometer, Bruker Optics, Gwangmyeng, Republic of Korea) was employed to confirm the interconnected bonding of the films. Thermal stability of the separator was assessed through thermogravimetric analysis (TGA, Universal V4.5A, TA instruments, Mettler Toledo, Columbus, OH, USA).

Results and Discussion

Neat HEC membranes exhibit high mechanical strength without the need for additional additives, yielding significant results in the gas flux method. An experiment was conducted to measure the permeance of a 200-µm HEC film is produced through a casting process using a gas-based method. After stabilizing the pressure at each level for 20 min, starting from 0.5 bar, formation of pores is observed. The same experiment was repeated by incrementally increasing the pressure by 0.5 bar.

As the film undergoes drying, the solvent's evaporation weakens intermolecular bonds within the previously solvent-occupied areas. HEC remains insoluble in organic solvents, leading to the formation of pores due to the weakened molecular bonds in regions where acetone, part of the solvent in which HEC dissolves, is present. These weakened areas experience pore formation under gas pressure, with variations in pore size and quantity based on pressure levels. Observations revealed a direct correlation between increased pressure and enhanced transport as shown in Table 1. Approximately 80 gas flux experiments were conducted to verify the reproducibility of this pressure-dependent transport, consistently demonstrating that transmittance increased with rising pressure (Scheme 1).

These findings suggest that the applied pressure becomes a determining factor for both the number and size of pores. Judging from that permeance is assessed by the pressure of gas to move in a straight path, the pores formed in the film also exhibit a linear arrangement.

Pores of approximately 20 µm were observed in the HEC films (Fig. 1b, c) using the gas flux process. In contrast, the film (Fig. 1a) that did not undergo the gas permeation method displayed a smooth surface with no discernible characteristics. This outcome indicates that pores are not solely generated due to solvent evaporation during drying; rather, they are only generated when the gas process is applied. Through the gas flux method, the film undergoes simultaneous drying and gas passage. This concurrent process results in the formation of pores, following the contours of the uneven surface depicted in Fig. 1. Since the permeance of the film is low, the pores observed in SEM are quite small. Consequently, when subjecting an HEC film to pressures exceeding a certain threshold, the size of the pores increases rather than the number of pores. This phenomenon can be attributed to the molecular structure of HEC, where the hydroxyl group is located on molecular chain, making it prone to bonding with a solvent. After drying, the solvent in these bonding sites evaporates, leading to pore formation.

Upon analyzing the molecular structure of HEC, we identified specific spectral peaks, notably the ether peak at 1052 to 1054 cm^{-1} and the hydroxyl group peak at 3417 to 3425 cm^{-1} in the FT-IR results. A comparative assessment of the peaks in HEC at 0 bar (Fig. 2a) and HEC at 1.5 bar (Fig. 2b) revealed no significant disparities. The evaluation of property changes was corroborated through SEM images, and the FT-IR data reaffirmed the absence of any chemical alterations. Consequently, it became evident that the sole modification influencing pore formation was of a physical nature.

Further examination of the chemical structure of HEC focused on verifying the ether functional group peak for precise analysis. Deconvolution techniques were employed

Table 1 Gas flux data of porous HEC

	GPU
Neat HEC at 2.5 bar	1.46 (±0.05)
Neat HEC at 3.0 bar	2.515 (±0.055)
Neat HEC at 3.5 bar	4.13 (±0.06)

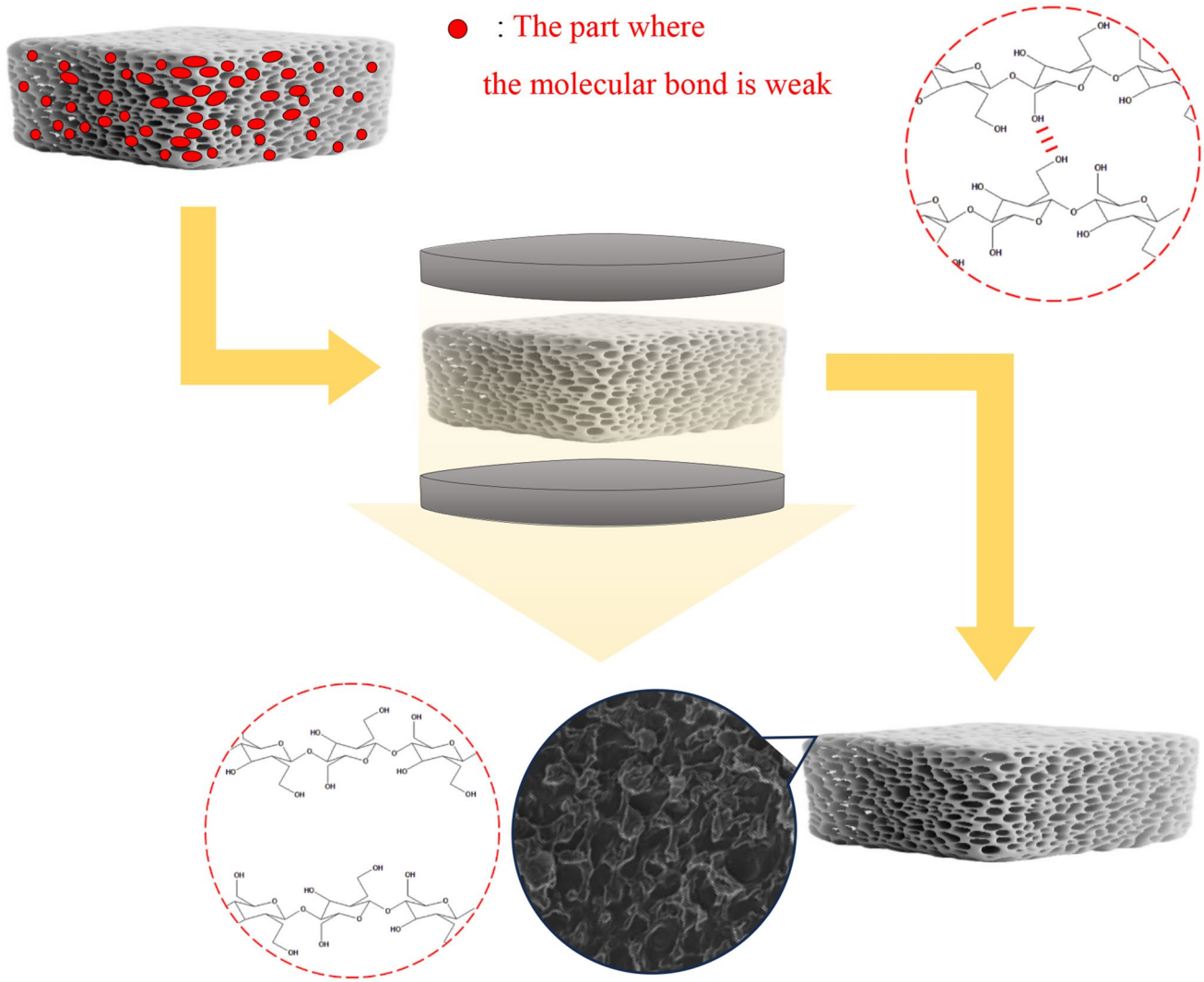

Scheme 1 Preparation process of the HEC separator

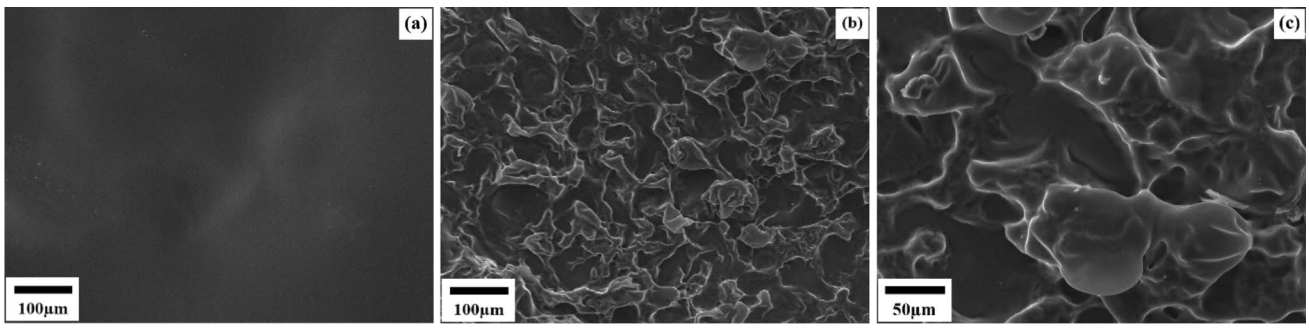

Fig. 1 SEM images of neat HEC film at 0 bar (**a**) and 1.5 bar (**b**, **c**)

to enhance accuracy by eliminating fine noise or fringes, yielding the results illustrated in Figs. 3 and 4. Notably, a pronounced peak corresponding to C–O stretching was observed in the pristine HEC membrane without the gas method applied. The deconvolved spectrum indicated the presence of three Gaussian centers, located at the

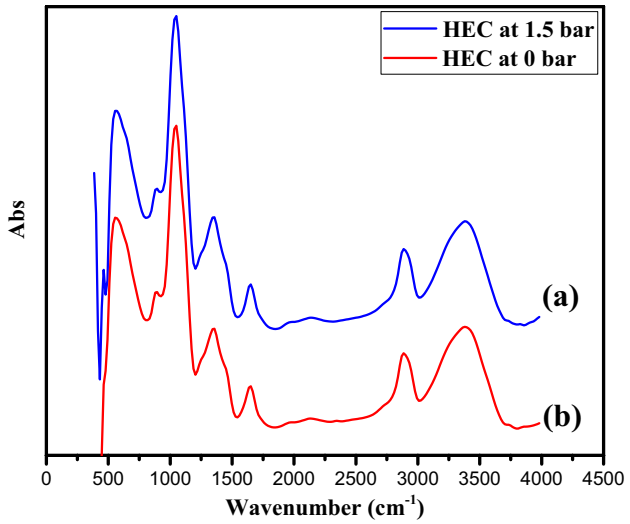

Fig. 2 FT-IR data: **a** HEC film at 0 bar and **b** HEC film exposed at 1.5 bar

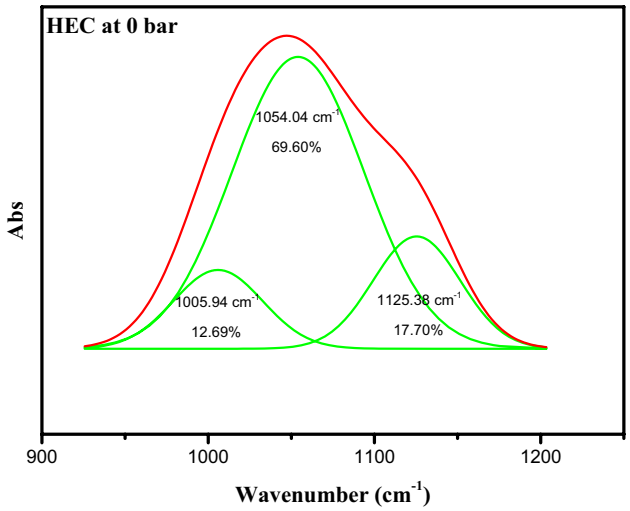

Fig. 3 FT-IR deconvoluted % of FT-IR data (ether functional group, a)

following wave numbers. Table 2 shows that the area ratios of these peaks were 12.69% at 1005.94 cm^{-1}, 69.60% at 1054.04 cm^{-1}, and 17.70% at 1125.38 cm^{-1}. Notably, the peak within the 1085–1050 cm^{-1} range is attributed to primary alcohol, while the region of 1150–1085 cm^{-1} indicates aliphatic ether.

To validate these findings, peak confirmation and deconvolution of the ether functional group in the Neat HEC separator obtained via the gas method at 1.5 bar were conducted. The resulting deconvolved spectrum revealed three Gaussian centers, along with their corresponding area ratios: 10.70% at 1004.91 cm^{-1}, 71.94% at 1052.81 cm^{-1}, and 17.38% at 1125.11 cm^{-1}. A comparative analysis with the results

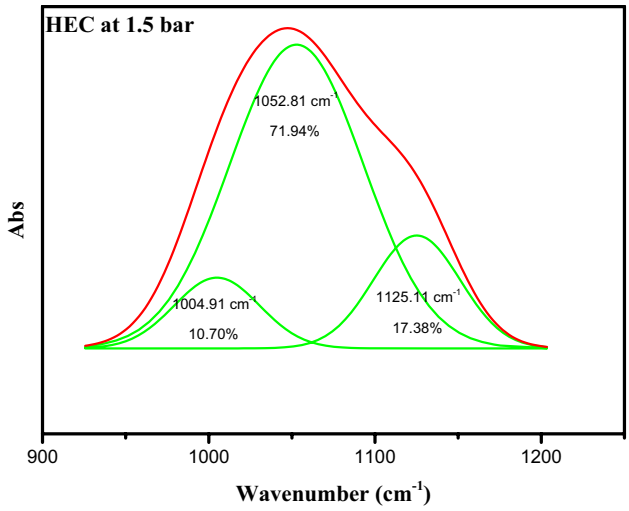

Fig. 4 FT-IR deconvoluted % of FT-IR data (ether functional group, b)

Table 2 Deconvoluted % of FT-IR data (ether functional group)

Peaks (cm^{-1})	HEC at 0 bar (%)	HEC at 1.5 bar (%)
1004 ~ 1006	12.69	10.70
1052 ~ 1054	69.60	71.94
1125	17.70	17.38

presented in Fig. 3 revealed no discernible alterations in peak position or area ratio of the Gaussian center, signifying the absence of any chemical changes related to the ether functional group.

The same analytical procedure was applied to assess the hydroxyl group. The wave numbers and area ratios corresponding to the three Gaussian centers of the deconvoluted FT-IR spectrum of the separator without the gas method were as follows: 35.24% at 3241.03 cm^{-1}, 60.61% at 3425.16 cm^{-1}, and 4.15% at 3577.95 cm^{-1}. Typically, the prominent and broad peak within the 3550–3200 cm^{-1} range signifies intermolecular bonded alcohol with O–H stretching.

The FT-IR spectrum of the hydroxyl group in the neat HEC separator, obtained using the gas method at 1.5 bar, was validated, followed by deconvolution analysis as shown in Figs. 5 and 6. Table 3 shows that the resultant deconvolved spectrum revealed three Gaussian centers and their corresponding area ratios: 32.81% at 3235.98 cm^{-1}, 61.20% at 3417.36 cm^{-1}, and 6.00% at 3569.19 cm^{-1}. A comparative assessment of the area ratios with those depicted in Figs. 5 and 6 revealed no discernible changes. This outcome signifies the absence of any chemical alterations concerning the

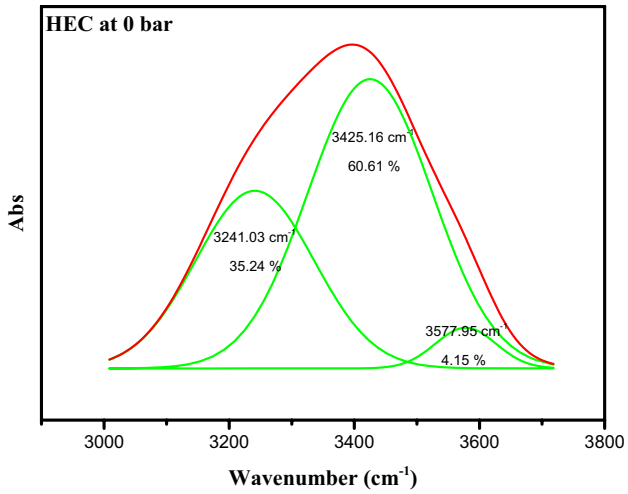

Fig. 5 FT-IR deconvoluted % of FT-IR data (hydroxyl group, a)

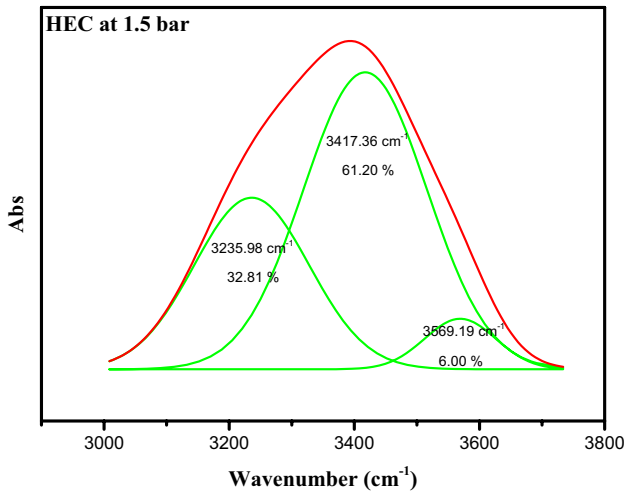

Fig. 6 FT-IR deconvoluted % of FT-IR data (hydroxyl group, b)

Table 3 Deconvoluted % of FT-IR data (hydroxyl group)

Peaks (cm^{-1})	HEC at 0 bar (%)	HEC at 0 bar (%)
3236 ~ 3241	35.26	32.81
3417 ~ 3425	60.61	61.20
3569 ~ 3578	4.15	6.00

hydroxyl group, akin to the observations for the ether functional group. Examination of HEC's functional group FT-IR spectra before and after the gas method further corroborated that solely pore formation occurred, without any associated chemical changes.

The TGA analysis graph exhibits distinct trends. A reduction in weight may occur due to several phenomena, including decomposition, resulting from the breakage of chemical bonds, as well as evaporation of volatile components at high temperatures and desorption of adsorbed substances. Conversely, weight gain may transpire due to interactions with the surrounding gas or the combination with oxygen or nitrogen in an oxidizing environment.

To evaluate thermal stability and the thermal life of the separator, various factors were considered via TGA and DTG analysis. It was noted that the trends in both graphs closely paralleled each other, particularly in relation to the gas permeation process, as illustrated in Fig. 7. During the heating process, two significant weight losses were observed in both the 0-bar and 3-bar films. In the initial stage, both films exhibited a slight percentage weight loss, which could be attributed to moisture evaporation, fine molecule separation, or volatilization. Subsequently, in the later reduction phase, a substantial reduction in weight was evident. This phenomenon was attributed to the chemical decomposition of HEC, with this phase being of paramount importance.

Importantly, it was observed that films subjected to the gas permeation process and featuring pore formation exhibited accelerated degradation. This discrepancy underscores alterations in the physical properties of these films, primarily stemming from the weakening of molecular bonds within the original film as pores developed. These results provide compelling evidence for the robust thermal stability of HEC films, even when exposed to temperatures exceeding 300 °C.

To distinctly compare the reduction phase of the two films, additional DGA representing the differential values of the TGA graph was conducted. The outcome reveals a similar temperature range for the decrease in both films, but notably, the gas-permeated film exhibits a faster reduction rate. This discrepancy in reduction rates between the gas-permeated and non-permeated films can be attributed to the method itself, illustrating the weakening of molecular interactions and the subsequent formation of pores as the underlying cause.

Conclusion

We succeed in preparing porous HEC polymer to have pores formed in the vertical direction without any additives by applying the gas pressure. Since no additives other than the solvent were introduced, the chemical properties remained unchanged in the FT-IR and TGA results. The disparities observed were solely attributed to variations in physical properties due to pore formation through the gas permeation process after drying. As evidenced by SEM images, pores approximately 20 μm in size were formed, conclusively established as originating from the gas permeation system. The analytical results confirm the absence of chemical property changes, with only alterations in mechanical strength

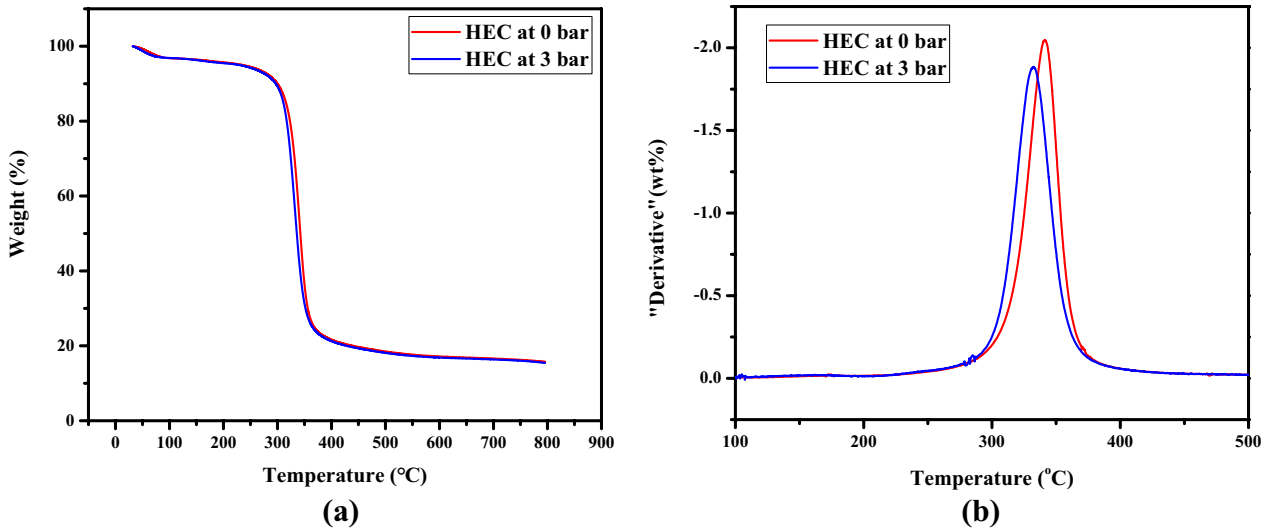

Fig. 7 **a** TGA data of neat HEC film at 0 bar and 3 bar and **b** DTG data of neat HEC film at 0 bar and 3 bar

and thermal stability observed. The high viscosity, robust mechanical strength owing to the HEC's chemical structure, and stability even at elevated temperatures exceeding 300 °C characterize it. Consequently, the results are economically valuable, as they signify that high stability and strength can be achieved without the need for additives.

Author Contributions HK collected the data and wrote the draft. SWK analyzed the data and reviewed the draft.

Funding This article is funded by 2022 Research Grant from Sangmyung University. (2022-A000-0054), Sang Wook Kang.

Data Availability Not applicable.

Declarations

Conflict of interest Not applicable.

References

1. W. Brown, D. Henley, J. Öhman, Macromol. Chem. Phys. **75**, 49 (1963)
2. A.A. Heidari, H. Mahdavi, Chem. Rec. **20**, 570 (2020)
3. C. Lee, S. Lee, S. W Kang, Carb. Polym. **324**, 121571 (2024)
4. D. Jahani, A. Nazari, M.Y. Panah, Korean J. Chem. Eng. **39**, 2099 (2022)
5. Y.K. Park, S.C. Jung, H.Y. Jung, Korean J. Chem. Eng. **40**, 91 (2023)
6. S.H. Kim, Y.R. Choi, Y.J. Cho, S.Y. Rhyu, S.W. Kang, Korean J. Chem. Eng. **38**, 1715 (2021)
7. X. Huang, J. Solid State Electrochem. **15**, 649 (2010)
8. J.-Q. Huang, Q. Zhang, Energy Storage Mater. **1**, 127 (2015)
9. X. Huang, Mater. Today **41**, 143 (2020)
10. J. Choi, J. Kim, Curr. Opin. Electrochem. **31**, 100858 (2022)
11. Y. Xiang, J. Li, Chemsuschem **9**, 3023 (2016)
12. H. Chen, Chem. Eng. J. **471**, 144593 (2023)
13. J. Zhang, ACS Appl. Mater. Interfaces **5**, 128 (2013)
14. E. Lizundia, Carbohydr. Polym. Technol. Appl. **1**, 100001 (2020)
15. S. Byun, Y. Cho, S. W. Kang, Int. J. Biol. Macromol. **254,** 127823 (2024)
16. A.M.A. Pistorius, W.J. DeGrip, Vib. Spectrosc. **36**, 89 (2004)
17. P. Laurson, AIP Adv. **10**, 085214 (2020)
18. M.Y. Zhang, Electrochim. Acta **245**, 752 (2017)
19. N. Saadatkhah, Can. J. Chem. Eng. **98**, 34 (2019)
20. N. Sun, T. Wang, X. Yan, Carbohydr. Polym. **172**, 49 (2017)
21. C. Cen, Int. J. Biol. Macromol. **231**, 123203 (2023)
22. F.H. Zulkifli, Int. J. Biol. Macromol. **122**, 562 (2019)
23. A. Mohammed, A. Abdullah, Proceedings of 2018 International Conference on Hydraulics and Pneumatics – HERVEX, (2018)
24. Y. Diao, Carbohydr. Polym. **169**, 92 (2017)
25. S. Zhong, Energy Storage Mater. **41**, 805 (2021)
26. D.C.N. Kung, S.W. Kang, J. Ind. Eng. Chem. **124**, 474 (2023)